HAL
open science

Turning a near-hovering controlled quadrotor into a 3D force effector

Guido Gioioso, Markus Ryll, Domenico Prattichizzo, Heinrich H. Bülthoff, Antonio Franchi

To cite this version:

Guido Gioioso, Markus Ryll, Domenico Prattichizzo, Heinrich H. Bülthoff, Antonio Franchi. Turning a near-hovering controlled quadrotor into a 3D force effector. IEEE Int. Conf. on Robotics and Automation (ICRA 2014), May 2014, Hong Kong, China. pp.6278 - 6284, 10.1109/ICRA.2014.6907785 . hal-01083777

HAL Id: hal-01083777

https://hal.science/hal-01083777

Submitted on 18 Nov 2014

HAL is a multi-disciplinary open access archive for the deposit and dissemination of scientific research documents, whether they are published or not. The documents may come from teaching and research institutions in France or abroad, or from public or private research centers.

L'archive ouverte pluridisciplinaire **HAL**, est destinée au dépôt et à la diffusion de documents scientifiques de niveau recherche, publiés ou non, émanant des établissements d'enseignement et de recherche français ou étrangers, des laboratoires publics ou privés.

Preprint version, final version at http://ieeexplore.ieee.org/ 2014 IEEE Int. Conf. on Robotics and Automation, Hong Kong, China

Turning a Near-hovering Controlled Quadrotor into a 3D Force Effector

Guido Gioioso[1,2], Markus Ryll[3], Domenico Prattichizzo[1,2], Heinrich H. Bülthoff[3] and Antonio Franchi[4,3]

***Abstract*— In this paper the problem of a quadrotor that physically interacts with the surrounding environment through a rigid tool is considered. We present a theoretical design that allows to exert an arbitrary 3D force by using a standard near-hovering controller that was originally developed for contact-free flight control. This is achieved by analytically solving the nonlinear system that relates the quadrotor state, the force exerted by the rigid tool on the environment, and the near-hovering controller action at the equilibrium points, during any generic contact. Stability of the equilibria for the most relevant actions (pushing, releasing, lifting, dropping, and left-right shifting) are proven by means of numerical analysis using the indirect Lyapunov method. An experimental platform, including a suitable tool design, has been developed and used to validate the theory with preliminary experiments.**

I. INTRODUCTION

Over the past decade, Unmanned Aerial Vehicles (UAVs) attracted an increasing interest in the robotics community, due to their versatility and to the many potential indoor and outdoor applications, including, e.g., landscape survey, surveillance and reconnaissance, manufacturing and logistics automation. In this context UAVs have been mainly considered as flying sensors rather than flying actuators, and the possibility of using flying robots for mobile manipulation, i.e., enabling physical interaction with the surrounding environment, has not been sufficiently investigated yet. In fact, designing novel flying robotic systems able to perform this kind of interaction would open a much wider range of possible applications in the aerial robotics field.

Among the UAV platforms, the quadrotor gained a lot of popularity in the robotic community, due to its mechanical simplicity and robustness. Being able to hover and perform vertical take-off and landing, it represents also an ideal platform for developing and testing many new aerial manipulation concepts. In [1] a control law for a quadrotor equipped with a rigid tool is proposed and tested in simulation. The controller is based on feedback linearization thus requiring for a rather precise knowledge of the system mechanical parameters and state estimation that is sometime hard to find in real application scenarios. Furthermore, some caution is needed when dealing with a possible unstable zero dynamics. A passivity-based controller is presented in [2] for a quadrotor endowed with a delta-shaped manipulator. Using a decoupled approach the actuation of the manipulator is employed to apply forces on a wall relying on the fact that the flight controller is able to keep steady the UAV position during contact. The authors in [3] present a hybrid framework with the goal of letting the quadrotor follow a desired trajectory while exerting a force on the environment. The approach relies on the empirical identification of a map that relates the exerted measured wrench with the thrust and torque inputs of the used quadrotor platform. In [4] a control framework is presented that allows the one-dimensional manipulation of a cart performed by one or two quadrotors through a rigid tool. In [5] a framework for robust control of a UAV for docking-undocking operation on a vertical surface based on a path following strategy is developed and tested in simulation. A recent work [6] proposes an interaction and damping assignment passivity-based controller (IDA-PBC) that is able to change the apparent dynamical parameters of a quadrotor. The authors have shown that this controller can be successfully used to shape the dynamical behavior of a quadrotor when in contact with a physical environment. Finally, studying the physical interaction with the environment is essential for applications in which UAVs are used as mobile manipulating platforms, see, e.g., [7], [8].

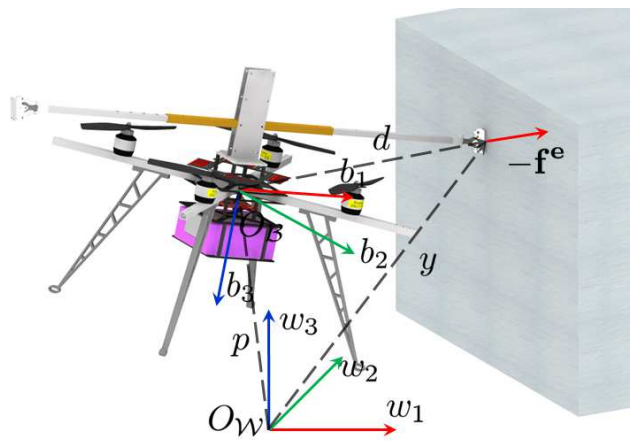

Fig. 1: CAD model of the quadrotor setup developed and used for our experiments and main frames and symbols used to model it.

In this paper we theoretically formulate the problem of controlling a quadrotor UAV endowed with a rigid tool whose tip has to be used in order to exert a prescribed 3D force on the environment. This is a basic task whose study may be instrumental for more complex manipulation behav-

[1]Department of Information Engineering and Mathematics, University of Siena, via Roma 56, 53100 Siena, Italy [gioioso, prattichizzo]@dii.unisi.it

[2]Department of Advanced Robotics, Istituto Italiano di Tecnologia, via Morego 30, 16163 Genova, Italy

[3]Max Planck Institute for Biological Cybernetics, Dept. of Human Perception, Cognition and Action, Spemanstr. 38, 72076, Tübingen, Germany [markus.ryll,hhb]@tuebingen.mpg.de

[4]Centre National de la Recherche Scientifique (CNRS), Laboratoire d'Analyse et d'Architecture des Systèmes (LAAS), 7 Avenue du Colonel Roche, 31077 Toulouse CEDEX 4, France. antonio.franchi@laas.fr

ior performed by a single or multiple UAVs. The advantage of this approach is to obtain a structure that is light-weight, mechanically simple and with a larger time autonomy than a single bulky UAV equipped with a manipulator with several DOFs. Moreover, a system with multiple UAVs endowed with simple tools might result even more effective and versatile as shown, e.g., in [9] where it is presented the control of a flying hand constituted by multiple simple UAVs each one acting as a single finger.

The model of a quadrotor endowed with a rigid tool is introduced in Sec. II along with a control law suitable for force exertion. The control scheme is based on the near-hovering linearizing control approach that is commonly used for contact-free flight on many quadrotor UAV platforms. The adoption of a widely used control law is the main strength of this approach, which brings many advantageous consequences: i) our solution can be easily applied by other research labs by slightly adapting the built-in controller that is already present on their platform; ii) the same controller is used both for the free flight phase and for the contact phase thus being exempt from the need for exact contact detection and switching-related problems; iii) despite being conceived for a near-hovering contact-free flight, during contact the controller can be used with high tilt angles; furthermore, iv) the control law is based neither on full cancellation, as feedback linearization, nor on sliding surfaces, thus it is expected to have a robust behavior in real world conditions.

By virtue of the analytical study carried-out in Sec. III on the nonlinear equilibria of the controlled system, the controller can be effectively used to apply, at steady state, any given 3D contact force at the contact point. Stability of the controlled system at the equilibria corresponding to the given forces is numerically proven in Sec. IV for the most important interaction cases, such as pushing, releasing, lifting, dropping, and left/right shifting.

The implementation of an experimental platform which includes the design of a tool that can be easily mounted on a quadrotor to establish contact with the environment, is presented in Sec. V where a preliminary experiment in the dynamic case (i.e., time-varying force profile) is also shown. Section VI concludes the paper and presents future developments of this work.

II. MODEL AND STANDARD NH CONTROLLER

In this section we present the notation used throughout the paper while briefly introducing the standard quadrotor dynamical model. Refer to Fig. 1 for an illustration. An inertial world frame $\mathscr{W}:\{O_{\mathscr{W}},\vec{w}_1,\vec{w}_2,\vec{w}_3\}$ and a quadrotor body frame $\mathscr{B}:\{O_{\mathscr{B}},,\vec{b}_1,\vec{b}_2,\vec{b}_3\}$ are considered. The origin of the body frame is coincident with the center of mass of the quadrotor which is also the geometric center of the four propellers. We indicate with $\mathbf{p}=(p_1,p_2,p_3)^T\in\mathbb{R}^3$ the position of $O_{\mathscr{B}}$ in $\mathscr{W}$ and with $\mathbf{v}=(v_1,v_2,v_3)^T\in\mathbb{R}^3$ the corresponding linear velocity. The scalar $m\in\mathbb{R}$ denotes the mass of the quadrotor and $\mathbf{J}\in\mathbb{R}^{3\times3}$ its inertia matrix with respect to the body frame. Finally, let $\mathbf{R}\in\mathbb{R}^{3\times3}$ represent the rotation matrix from the body frame to the inertial world frame and $\omega\in\mathbb{R}^3$ be the angular velocity vector that represents the rotation of $\mathscr{B}$ with respect to $\mathscr{W}$, expressed in $\mathscr{B}$. The orientation of the quadrotor is represented by $\eta:=(\phi,\theta,\psi)^T\in\mathbb{R}^3$, with ϕ,θ,ψ being respectively the roll, pitch and yaw angles (RPY). The rotation matrix can be written using RPY as $\mathbf{R}(\eta)=\mathbf{R_z}(\psi)\mathbf{R_y}(\theta)\mathbf{R_x}(\phi)$, where $\mathbf{R_x},\mathbf{R_y},\mathbf{R_z}$ are the elementary rotation matrices about the three coordinate axis.

As common practice in literature we assume as control inputs the total thrust acting on the $-\vec{b}_3$ direction, denoted with $\lambda\in\mathbb{R}^+$, and the total moment expressed in $\mathscr{B}$, denoted with $\tau=(\tau_1,\tau_2,\tau_3)^T\in\mathbb{R}^3$. Being the four inputs less than six (the number of configuration parameters $\mathbf{p},\eta$) the quadrotor is an underactuated system. Nevertheless its actuation is enough to exert any 3D force on the environment.

We assume that the quadrotor is equipped with a tool whose tip position in body frame is expressed by the constant vector $\mathbf{d}=(d_x,d_y,d_z)^T\in\mathbb{R}^3$. Without loss of generality we take $\vec{b}_2$ aligned with the projection of the tool on the plane spanned by $\vec{b}_1$ and $\vec{b}_2$, thus resulting in $d_y=0$. Let $\mathbf{y}\in\mathbb{R}^3$ be the position of the tool-tip in the world frame:

$$\mathbf{y}=\mathbf{p}+\mathbf{R}\mathbf{d}. \tag{1}$$

The environment interacts with the quadrotor by exerting a force $\mathbf{f^e}\in\mathbb{R}^3$ on the tool-tip, which is expressed in the world inertial frame. The interaction moment at the tool-tip is assumed negligible. This assumption is widely used in literature and it is referred to as hard finger contact model [10]. Under these assumptions, the equations of motion of the quadrotor can be written as:

$$\dot{\mathbf{p}}=\mathbf{v} \tag{2}$$

$$m\dot{\mathbf{v}}=-\lambda\mathbf{R}\hat{\mathbf{z}}+mg\hat{\mathbf{z}}+\mathbf{f^e} \tag{3}$$

$$\dot{\eta}=\mathbf{T}(\eta)\omega \tag{4}$$

$$\mathbf{J}\dot{\omega}=-\omega\times\mathbf{J}\omega+\tau+\mathbf{d}\times\mathbf{R}^T\mathbf{f^e}, \tag{5}$$

where $\hat{\mathbf{z}}=(0,0,1)^T$ and $\mathbf{T}(\eta)\in\mathbb{R}^{3\times3}$ transforms ω to the RPY rates $\dot{\eta}$.

In the following we adopt the common assumption that the quadrotor is never in a singular configuration (i.e., $\phi=\theta=0$), in fact if this happens, the total thrust λ cannot be used to counterbalance the gravity force, thus consisting in a useless case for our purposes.

A. Standard Near-hovering Controller

In this section we revise a control law that has been widely used in literature (see, e.g., [11], [12], [13]) to perform near-hovering and contact-free trajectory tracking. Even though this controller is well known in literature, it is essential to recall its main structure and notation for the following Sec. III where we will show how this controller can be effectively used to perform a contact force on the environment even in far-hovering conditions.

An inner-loop PID controller tracks some desired RPY angles $\eta_{\mathbf{d}}=(\phi_d,\theta_d,\psi_d)^T\in\mathbb{R}^3$, relying on the fact that the

rotational dynamics is fully actuated. In fact, differentiating (4) and substituting (5), we get

$$\ddot{\eta} = \mathbf{T}(\eta)\mathbf{J}^{-1}(-\omega \times \mathbf{J}\omega + \tau + \mathbf{d} \times \mathbf{R}^T\mathbf{f}^{\mathbf{e}}) + \dot{\mathbf{T}}(\eta)\omega.$$

The PID attitude regulation controller is thus defined as:

$$\tau = \mathbf{J}\mathbf{T}^{-1}(\eta)\mathbf{K}_A\eta_{\mathbf{e}} \tag{6}$$

where:

$$\mathbf{K}_A^T = \begin{bmatrix} k_{DA}^{\phi} & 0 & 0 \\ k_{PA}^{\phi} & 0 & 0 \\ k_{IA}^{\phi} & 0 & 0 \\ 0 & k_{DA}^{\theta} & 0 \\ 0 & k_{PA}^{\theta} & 0 \\ 0 & k_{IA}^{\theta} & 0 \\ 0 & 0 & k_{DA}^{\psi} \\ 0 & 0 & k_{PA}^{\psi} \\ 0 & 0 & k_{IA}^{\psi} \end{bmatrix}, \quad \eta_{\mathbf{e}} = \begin{bmatrix} -\dot{\phi} \\ \phi_d - \phi \\ \int(\phi_d - \phi)\,\mathrm{d}t \\ -\dot{\theta} \\ \theta_d - \theta \\ \int(\theta_d - \theta)\,\mathrm{d}t \\ -\dot{\psi} \\ \sin(\psi_d - \psi) \\ \int \sin(\psi_d - \psi)\,\mathrm{d}t \end{bmatrix} \tag{7}$$

that leads to the closed-loop dynamics:

$$\ddot{\eta} + \mathbf{K}_A\eta_{\mathbf{e}} = \mathbf{T}\mathbf{J}^{-1}(-\omega \times \mathbf{J}\omega + \mathbf{d} \times \mathbf{R}^T\mathbf{f}^{\mathbf{e}}) + \dot{\mathbf{T}}\omega.$$

It has been shown that, in contact-free flight and under suitable conditions of the initial state and gain selection, $(\eta_{\mathbf{e}}, \dot{\eta}_{\mathbf{e}})$ is locally exponentially stable.

Since in contact-free flight this controller is meant to work in near hovering $\mathbf{T}^{-1}(\eta)$ can be approximated by a 3×3 identity matrix in (6). Furthermore, assuming that the $\mathbf{J}$ is diagonal, as common practice, we can hide $\mathbf{J}$ in the gain matrix $\mathbf{K}_A$ thus obtaining a simpler expression for τ:

$$\tau = \mathbf{K}_A\eta_{\mathbf{e}}. \tag{8}$$

Note that even if the previous ones seem crude approximations, they have been proven to work very well in reality, see the previously cited work, when the task is to fly in near hovering. Furthermore, we are not interested in having excellent performances in free flight since our focus is in the contact case.

An outer-loop controller is then designed by choosing the thrust such as to actuate the vertical dynamics

$$\lambda = -\frac{m}{\cos\phi\cos\theta}(-g - b_P^z v_3 + k_{PP}^z e_3) \tag{9}$$

where b_P^z and k_{PP}^z are two positive scalar gains and e_3 is an additional control input. Secondly, in order to act on the horizontal dynamics, the desired roll ϕ_d and pitch θ_d are set such that

$$\begin{pmatrix} \sin\phi_d \\ \sin\theta_d \end{pmatrix} = \frac{m}{\lambda}\begin{pmatrix} -s_\psi & c_\psi \\ -c_\psi/c_\phi & -s_\psi/c_\phi \end{pmatrix}\begin{pmatrix} -b_P v_1 + k_{PP}e_1 \\ -b_P v_2 + k_{PP}e_2 \end{pmatrix} \tag{10}$$

where e_1, e_2 are two additional control inputs, and $s_\bullet$ and $c_\bullet$ denote $sin(\bullet)$ and $cos(\bullet)$ respectively. The interested reader is referred to [13] for the analytical derivation of (10). We gather the three additional control inputs in the vector $\mathbf{e} = (e_1, e_2, e_3)^T \in \mathbb{R}^3$.

Remark 1: (Behavior in contact-free flight) In the literature the controller (8),(9),(10) has been used to steer the robot during contact-free (i.e., $\mathbf{f}^{\mathbf{e}} = \mathbf{0}$) motion. In fact, simply speaking, if we plug (9) in the third row of (3) we obtain

$$m\dot{v}_3 = -b_P^z v_3 + k_{PP}^z e_3, \tag{11}$$

furthermore, if the attitude controller is fast enough, i.e., s.t. $\theta \simeq \theta_d$ and $\phi \simeq \phi_d$, the first two rows of (3) become (see [13])

$$m\begin{pmatrix} \dot{v}_1 \\ \dot{v}_2 \end{pmatrix} \simeq \begin{pmatrix} -b_P v_1 + k_{PP}e_1 \\ -b_P v_2 + k_{PP}e_2 \end{pmatrix}$$

Therefore, one can choose $\mathbf{e} = \mathbf{p_d} - \mathbf{p}$ in order to exponentially regulate $\mathbf{p}$ to a desired constant position $\mathbf{p_d}$.

III. NONLINEAR EQUILIBRIA DURING CONTACT

Departing from the assumption that is commonly done in the literature when dealing with such controller (see Remark 1) in this paper we consider the case when $\mathbf{f}^{\mathbf{e}} \neq 0$ and possibly $\theta \neq \theta_d$ and $\phi \neq \phi_d$. To this aim in this section we analytically derive the equilibria of the closed loop system (2)–(5) subject to control (8),(9),(10). In particular we are interested in the static nonlinear relationship between $-\mathbf{f}^{\mathbf{e}}$, i.e., the force exerted at the equilibrium by the quadrotor on the environment through the tool-tip, and $\mathbf{e}$, i.e., the 3D control input that is left free by the controller described in Sec. II. The goal of the following analysis will be to find $\mathbf{e}$ given a desired $-\mathbf{f}^{\mathbf{e}}$. The equations to be solved in order to find the sought relation can be obtained by writing (3),(5),(8),(9),(10) at the equilibrium (i.e., $\mathbf{v} = \dot{\mathbf{v}} = \omega = \dot{\omega} = \mathbf{0}$). This results in the following nonlinear system of 12 scalar equations

$$-\lambda\mathbf{R}\hat{\mathbf{z}} + mg\hat{\mathbf{z}} + \mathbf{f}^{\mathbf{e}} = 0 \tag{12}$$

$$\tau + \mathbf{d} \times \mathbf{R}^\top\mathbf{f}^{\mathbf{e}} = 0 \tag{13}$$

$$\tau - \mathbf{K_A}\eta_{\mathbf{e}} = 0 \tag{14}$$

$$\lambda c_\theta c_\phi - mg + k_{PP}e_3 = 0 \tag{15}$$

$$\begin{pmatrix} s_{\phi_d} \\ s_{\theta_d} \end{pmatrix} - \frac{mk_{PP}}{\lambda}\begin{pmatrix} -s_\psi & c_\psi \\ -c_\psi/c_\phi & -s_\psi/c_\phi \end{pmatrix}\begin{pmatrix} e_1 \\ e_2 \end{pmatrix} = 0 \tag{16}$$

where the 12 unknowns are the sought e_1, e_2, e_3, together with $\phi, \theta, \psi, \phi_d, \theta_d, \lambda, \tau_1, \tau_2, \tau_3$. The admissible values of the variables are $\phi, \theta \in (-\frac{\pi}{2}, \frac{\pi}{2})$, $\psi \in (-\pi, \pi)$, and $\lambda > 0$. The known parameters are the external force components f_1^e, f_2^e, f_3^e, and $m, g, \mathbf{d}, \mathbf{K}_A, k_{PP}$ and ψ_d.

A. Total thrust λ and e_3

Equation (12) can be rewritten as:

$$f_1^e = \lambda(c_\psi c_\phi s_\theta + s_\psi s_\phi) \tag{17}$$

$$f_2^e = \lambda(c_\phi s_\psi s_\theta - s_\phi c_\psi) \tag{18}$$

$$f_3^e + mg = \lambda c_\theta c_\phi \tag{19}$$

from which it descends, after some straightforward algebra, that the total thrust must be:

$$\lambda = \sqrt{(f_1^e)^2 + (f_2^e)^2 + (f_3^e + mg)^2}. \tag{20}$$

Moreover, using (19) and (15) the unknown e_3 can immediately be obtained as

$$e_3 = -\frac{f_3^e}{k_{PP}}. \tag{21}$$

B. RPY Angles ϕ,θ,ψ, desired roll/pitch ϕ_d,θ_d, and $e_1.e_2$

Operating the following change of variables:

$$x = c_\phi s_\theta \qquad y = s_\phi, \tag{22}$$

(17) and (18) can be rewritten as a linear system:

$$\begin{pmatrix} c_\psi & s_\psi \\ s_\psi & -c_\psi \end{pmatrix}\begin{pmatrix} x \\ y \end{pmatrix} = \frac{1}{\lambda}\begin{pmatrix} f_1^e \\ f_2^e \end{pmatrix} \tag{23}$$

that can be easily solved thus obtaining the following expressions for s_ϕ and s_θ

$$s_\phi = \frac{1}{\lambda}(f_1^e s_\psi - f_2^e c_\psi) \tag{24}$$

$$s_\theta = \frac{1}{\lambda c_\phi}(f_1^e c_\psi + f_2^e s_\psi). \tag{25}$$

Given the admissible values for ϕ,θ, it must be $c_\phi > 0$ and $c_\theta > 0$, therefore we have

$$c_\phi = +\sqrt{1-s_\phi^2} \tag{26}$$

$$c_\theta = +\sqrt{1-s_\theta^2}. \tag{27}$$

Substituting τ in (13) from (14), we obtain:

$$-\mathbf{K_A}\eta_\mathbf{e} = \mathbf{d}\times\mathbf{R}^\top\mathbf{f^e}. \tag{28}$$

Moreover, from equation (16) it is straightforward to express s_{ϕ_d} and s_{θ_d} as

$$s_{\phi_d} = \frac{mk_{PP}}{\lambda}(-s_\psi e_1 + c_\psi e_2) \tag{29}$$

$$s_{\theta_d} = \frac{mk_{PP}}{\lambda c_\phi}(-c_\psi e_1 - s_\psi e_2) \tag{30}$$

The system composed by (24),(25),(28),(29),(30) is thus made by 7 equations with 7 unknowns $\phi,\theta,\psi,\phi_d,\theta_d,e_2,e_3$.

From this point the solution changes depending on the values of the integral gains in $\mathbf{K}_A$.

1) No Integral Action ($k_{IA}^\phi = k_{IA}^\theta = k_{IA}^\psi = 0$): This is the most complex case. The third row of (28) is

$$K_{PA}s_{\psi_d-\psi} = -x[f_1(c_\psi s_\theta s_\phi - s_\psi c_\phi) + f_2(s_\psi s_\theta s_\phi + c_\psi c_\phi) + f_3 s_\phi c_\theta] \tag{31}$$

If $d_x = 0$ then $\psi = \psi_d$, and the solution for this case is given in Sec. III-B.2.

In the general case of $d_x \neq 0$ we first show how ϕ,θ,ψ can be separately found solving the subsystem formed by (24),(25),(31). In fact, plugging (24),(25),(26),(27) into (31), after some algebra, we obtain a trigonometric equation in which the only unknowns are s_ψ and c_ψ, i.e., the yaw ψ. Using the tangent half-angle substitution ($t_{\frac{\psi}{2}} = \tan(\frac{\psi}{2})$) the trigonometric equation that can be written as a 8-th order polynomial equation:

$$\begin{aligned}(\alpha^{(2)}+\alpha^{(7)})t_{\frac{\psi}{2}}^8 - 2(\alpha^{(4)}+\alpha^{(8)})t_{\frac{\psi}{2}}^7 - 4(\alpha^{(2)}-\alpha^{(5)}-\alpha^{(6)})t_{\frac{\psi}{2}}^6 - \\ 2(4\alpha^{(3)}-3\alpha^{(4)}+\alpha^{(8)})t_{\frac{\psi}{2}}^5 + 2(8\alpha^{(1)}+3\alpha^{(2)}-4\alpha^{(5)}+4\alpha^{(6)}-\alpha^{(7)})t_{\frac{\psi}{2}}^4 + \\ 2(4\alpha^{(3)}-3\alpha^{(4)}+\alpha^{(8)})t_{\frac{\psi}{2}}^3 - 4(\alpha^{(2)}-\alpha^{(5)}-\alpha^{(6)})t_{\frac{\psi}{2}}^2 + \\ 2(\alpha^{(4)}+\alpha^{(8)})t_{\frac{\psi}{2}} + \alpha^{(2)}+\alpha^{(7)} = 0\end{aligned} \tag{32}$$

where the coefficients are defined as follows:

$$\begin{aligned}
\alpha^{(1)} &= (k_\alpha f_1^e c_{\psi_d})^2; \quad \alpha^{(2)} = (k_\alpha f_2^e s_{\psi_d})^2 \\
\alpha^{(3)} &= -2k_\alpha^2 f_1^e c_{\psi_d}(f_1^e s_{\psi_d} + f_2^e c_{\psi_d}) \\
\alpha^{(4)} &= -2k_\alpha^2 f_2^e s_{\psi_d}(f_1^e s_{\psi_d} + f_2^e c_{\psi_d}) \\
\alpha^{(5)} &= k_\alpha^2[(f_1^e s_{\psi_d})^2 + (f_2^e c_{\psi_d})^2 + 4f_1^e f_2^e s_{\psi_d} c_{\psi_d}] \\
\alpha^{(6)} &= a_\alpha^2 - (k_\alpha\lambda c_{\psi_d})^2; \; \alpha^{(7)} = b_\alpha^2 - (k_\alpha\lambda s_{\psi_d})^2 \\
\alpha^{(8)} &= 2a_\alpha b_\alpha + 2(k_\alpha\lambda)^2 s_{\psi_d} c_{\psi_d}
\end{aligned}$$

and

$$a_\alpha = f_1^{e3} + f_1^e f_2^{e2} - f_1^e\lambda^2 + f_1^e f_3^{e2} + f_1^e f_3^e mg$$

$$b_\alpha = -f_2^{e3} - f_1^{e2} f_2^e + f_2^e\lambda^2 + f_2^e f_3^{e2} + f_2^e f_3^e mg, \quad k_\alpha = \frac{-\lambda k_{PA}}{d_x}.$$

The real solutions of (32), that are efficiently found numerically, represent only candidate solutions for ψ, since some of them hold for negative values of c_θ and c_ϕ, which are not allowed in our setting. In order to prune the candidates it is then sufficient to plug them in (24),(25),(26),(27) and validate the found values by substitution in (31).

The variables ϕ_d and θ_d can be then computed from the first two rows of (28) and from the knowledge of ϕ,θ,ψ:

$$\phi_d = \phi + \frac{d_z}{k_{PA}^\phi}[f_1^e(c_\psi s_\theta s_\phi - c_\phi s_\psi) + f_2^e(s_\psi s_\theta s_\phi + c_\phi c_\psi) + f_3^e s_\psi c_\theta] \tag{33}$$

$$\begin{aligned}\theta_d = \theta - \frac{d_z}{k_{PA}^\theta}[f_1^e(c_\theta c_\psi) + f_2^e(s_\psi c_\theta) - f_3^e s_\theta] + \\ \frac{d_x}{k_{PA}^\theta}[f_1^e(c_\psi c_\phi s_\theta + s_\theta s_\psi) + f_2^e(s_\psi c_\phi s_\theta - s_\phi c_\psi) + f_3^e c_\theta c_\phi]\end{aligned} \tag{34}$$

Finally, from (29),(30) it is easy to obtain

$$e_1 = \frac{\lambda}{mk_{PP}}(-s_\psi s_{\phi_d} - c_\psi s_{\theta_d} c_\phi) \tag{35}$$

$$e_2 = \frac{\lambda}{mk_{PP}}(c_\psi s_{\phi_d} - s_\psi s_{\theta_d} c_\phi). \tag{36}$$

Fig. 2 shows the evolution of e_1,e_2,e_3 in this case, depending on f_1,f_2,f_3 for typical values of the mechanical and control parameters and $\psi_d = 0$.

2) Integral Action only on ψ ($k_{IA}^\phi = k_{IA}^\theta = 0$, $k_{IA}^\psi > 0$): In this case, because of the integral action, at the equilibrium we have that

$$\psi = \psi_d. \tag{37}$$

Therefore $\phi,\theta,\phi_d,\theta_d$ can be computed directly by plugging (37) in (24),(25),(26),(29),(30). Finally, as in the previous case, e_1,e_2 are obtained from (35) and (36), respectively.

3) Integral Action on ϕ and θ ($k_{IA}^\phi > 0, k_{IA}^\theta > 0$, k_{IA}^ψ any): In this case the values of ψ,ϕ and θ can be computed as per Sec. III-B.1 or as per Sec. III-B.2, depending on the value of k_{IA}^ψ (either equal or greater than zero). Then, because of the integral actions, at the equilibrium we have $\phi = \phi_d$

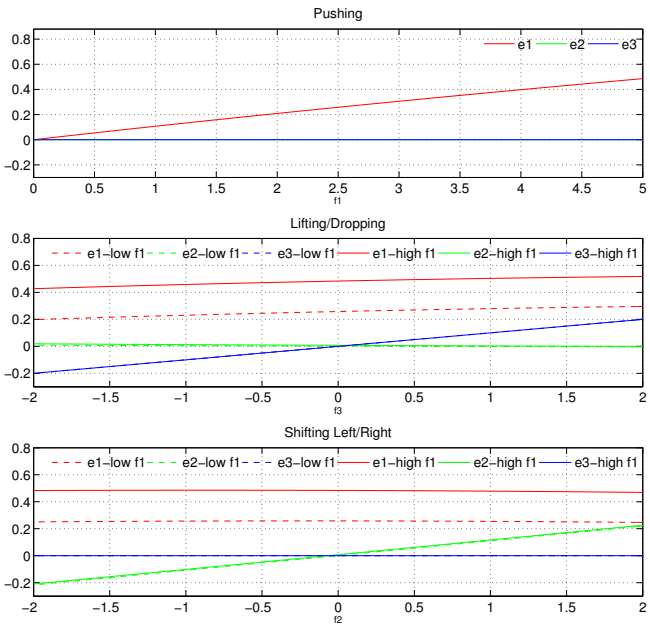

Fig. 2: Evolution of e_1, e_2, e_3 depending on f_1, f_2, f_3 [N] in the case of 'no integral action'.

and $\theta = \theta_d$. Therefore, equating the rhs of (24) with the rhs of (29) and the rhs of (25) with the rhs of (30) we obtain:

$$e_1 = -\frac{f_1^e}{mk_{PP}} \qquad e_2 = -\frac{f_2^e}{mk_{PP}}. \tag{38}$$

C. Torques τ

In any case can be retrieved by using (14), i.e.,

$$\tau = -\mathbf{d} \times \mathbf{R}^\top \mathbf{f}^\mathbf{e}. \tag{39}$$

D. Short Discussion on the Equilibria

Let's observe the expressions of $\mathbf{e}$ as function of the desired force $-\mathbf{f}^e$ and the desired yaw ψ_d that we found in the three different cases considered in Sec. III-B.1, III-B.2 and III-B.3. First it can be observed that an analytical expression in closed-form can be written only when at least some integral actions are considered, while it must be numerically computed when $k_{IA}^\phi = k_{IA}^\theta = k_{IA}^\psi = 0$. Moreover, in all the cases the value of e_3 only depends on the value of f_3^e while this decoupling property holds for e_1 and e_2 only in the third case (where $k_{IA}^\phi > 0, k_{IA}^\theta > 0$, k_{IA}^ψ any). In this last case it can be also observed that the value of $\mathbf{e}$ does not depend on the position $\mathbf{d}$ of the tool-tip in body frame.

IV. STABILITY OF THE EQUILIBRIUM POINTS

This section presents a numerical stability analysis for the equilibrium points defined in Sec. III using the indirect Lyapunov method for the case of 'no integral action'. We plan to address the remaining cases in a future work. The dynamical system defined by (3),(4),(5) subject to control (8),(9),(10) can be interpreted as nonlinear system $\dot{x} = f(x,u)$ with state $x = (p, v, \eta, \omega)$ and inputs $u = (e, \psi_d)$. In Sec. III we found how to efficiently compute the equilibrium (x_e, u_e) for any given external force $\mathbf{f}^\mathbf{e}$. It is therefore possible to compute the Jacobian matrix $\frac{\partial f}{\partial x}$ in (x_e, u_e) and efficiently check its eigenvalues. Negativeness of the largest real part of all the eigenvalues implies local asymptotical stability of the equilibrium (x_e, u_e) for the nonlinear system [14].

To this aim, we numerically computed the eigenvalues of the Jacobian matrix considering reasonable values for the system parameters and letting $\mathbf{f}^e, \psi_d$ and $\mathbf{d}$ vary over the domains of interest. In particular, we set $m = 1\,\text{kg}$, $\mathbf{J} = \text{diag}\{0.13, 0.13, 0.22\}\,\text{kg}\cdot\text{m}^2$, $k_{PP} = 10$ $b_P = 9$, $k_{PP}^z = 10$, $b_P^z = 9$, $k_{PA}^\phi = k_{PA}^\theta = k_{PA}^\psi = 12$, $k_{DA}^\phi = k_{DA}^\theta = k_{DA}^\psi = 7$. All the integral gains of the position and the attitude controller were set to zero. In all these cases we also set $\psi_d = 0$. and consider all the possible positions of the tool-tip d according to the design described in Sec. V-A, i.e., $d_x \in \{0.25, 0.27, 0.29, 0.31, 0.33, 0.35\}$ and $d_z \in \{-0.14, -0.11, -0.08, -0.05, 0.5, 0.8, 0.11, 0.14\}$ (we recall that we assumed, without loss of generality, $d_y = 0$). The forces are sampled considering five clusters that cover typical interaction cases such as pure pushing/releasing, lifting/dropping while pushing with low and high pushing force, and shifting left/right while pushing with low and high pushing force. Each of the five plots of Fig. 3 shows the evolution of the largest real part within each of the five clusters for every considered value of d_x and d_z. It is possible to see that in all the cases in exam the largest real part is negative thus resulting in a Hurwitz $\frac{\partial f}{\partial x}$ and, consequently, in a locally asymptotically stable equilibria for the nonlinear system. We now analyze more in detail each considered case.

1) Pushing/Releasing: In this cluster (first plot in Fig. 3) f_1^e has been regularly sampled from 0 N to -5 N with a sampling step 0.01 N while f_2^e and f_3^e have been keep equal to zero. Since $\psi^d = 0$, this corresponds to the case in which the quadrotor is performing a frontal pushing on the environment with pushing force $-f_1^e$. In every case a smaller d_x corresponds to a larger absolute value of the real part. This behavior is more evident when $d_z > 0$, i.e., the tool-tip is placed below the Center of Mass (CoM). The absolute value is constant w.r.t. d_z when $d_z > 0$ and monotonically decreasing w.r.t. d_z when $d_z < 0$.

2) Lifting/Dropping while Pushing: In these two clusters (second and third plots of Fig. 3) f_3^e is sampled between 0 N to 2 N with sampling step 0.01 N and two different (constant) values are considered for f_1^e, corresponding to a low (-2.5 N) and a high (-5 N) pushing force, respectively. The component f_e^3 is kept equal to zero. The trends w.r.t. to d_x and d_z are qualitatively comparable to the pure pushing case.

3) Shifting Left/Right while Pushing: In these two last clusters (fourth and fifth plots of Fig. 3) f_2^e is regularly sampled from -2 N to 2 N with a sampling step 0.01 N. The frontal pushing force f_1^e takes, as in the previous case, two different constant values (soft and hard pushing) and f_e^3 is kept equal to zero. Since $\psi_d = 0$ this corresponds to the case in which the quadrotor has to perform a lateral shift of the tooltip. It is interesting to note that in the case of low pushing force, basically d_z does not affect the largest real part. Dependency from the distance d_x is in accordance with

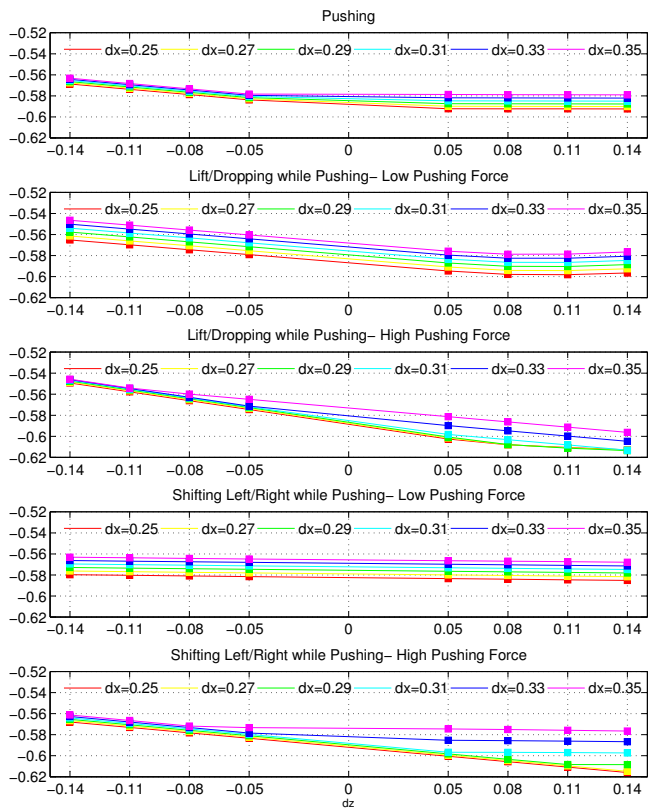

Fig. 3: Stability of the linearized systems. Each square in the plots represents the largest real part of the eigenvalues of $\frac{\partial f}{\partial x}$ when $\mathbf{f^e}$ is sampled along relevant interaction force trajectories (clusters) for certain values of d_z and d_x.

the previous analyzed cases. Concerning the trend when $f_1^e =$ -5 N we see that dependency from d_x becomes relevant only when $d_z > 0$ (tooltip below the CoM).

V. PRELIMINARY EXPERIMENTS

To further validate the theoretical and numerical analysis we developed an experimental setup that includes a in-house developed quadrotor (described in Sec. V-A), a Six-Axis force torque sensor 'Gamma' by ATI and an external motion capture system aimed at tracking the position and orientation of the quadrotor (see Fig. 1 for the CAD model and Fig. 5 for its implementation). In this Sec. V-B we report the outcome of a preparatory experiment that is designed to approximately perform a pushing and releasing maneuver.

A. Quadrotor and Tool Design

The quadrotor used to perform the experiments is based on the MK-Quadro MikroKopter platform. The overall mass including the tool is 1.2 kg. To increase the agility and decrease the size of the quadrotor we decided to use 20 *cm* diameter propellers. The overall diameter between two opposing propeller axis is $l = 0.314$ *m*. The distance vector between the tool-tip and the quadrotor body frame in performed experiment is $\mathbf{d} = (0.334, 0.0, 0.056)$ m. A copy of the tool was mounted on the opposite side in order to balance the weight of the one actually used to apply force on

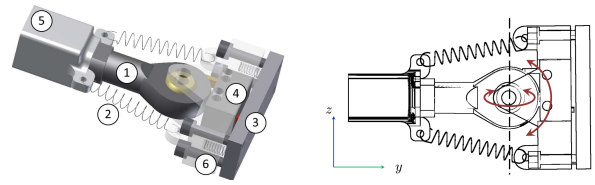

Fig. 4: Left: CAD picture of tool tip: 1. Gimbal bearing, 2. Springs to stabilize gimbal, 3. End effector plate, 4. Micro switch, 5. Connection to quadrotor, 6. Springs to bring back the plate in rest position when not in contact; Right: Schematic side view of tool tip presenting the degrees of freedom of the tool tip.

the sensor (see Fig. 1). The tool tip end effector (see Fig. 4) includes a gimbal bearing offering degrees of freedom in all the rotation axis (thus allowing the implementation of a hard finger contact). As it was mounted on our quadrotor, a big degree of freedom ($\pm 45°$) was offered around the pitch axis. To stabilize this degree of freedom a spring system is keeping the end effector tool-tip in the zero position when not in contact. Minor degrees of freedom ($\pm 15°$) are offered around the roll and yaw axis. The end effector tip additionally includes a micro switch that detects the contact.

B. Preliminary Result

In Fig. 5 a sequence of snapshots of the performed experiment is shown. The quadrotor equipped with the tool was remotely driven by a human operator to establish a contact with the surface. During the contact-free phase the operator commands a desired velocity to the UAV. During the contact phase the operator directly commands e_1, by means of a joystick, to let the pushing force applied by the robot on the surface follow approximately a trapezoidal profile (relying on the quasi-linear relation of Fig. 2 top). The results obtained during the experiments are plotted in Fig. 6. The plots refer only to the contact phase. It is easy to observe how the force applied by the quadrotor and read by the sensor follows the shape of the desired $\mathbf{e}$. Moreover the fingertip position remains practically constant during the experiment (no slippage occurs at the contact point). Finally in Fig. 7 the linear relationship between the applied pushing force and the signal e_1 commanded by the operator is plotted. The expected hysteresis is due to the fact that it is almost impossible for a human operator to fulfill the quasi-staticity of the motion due to the coarse control over e_1 allowed by a small joystick. For the same reason, the increasing and the decreasing phases are clearly asymmetric in Fig. 6. The reader is encouraged to watch the video attached to this submission in which the preliminary experiment is shown.

VI. CONCLUSIONS AND FUTURE WORK

In this paper we presented a control design that allows a quadrotor to exert a desired 3D contact force on a surface through a tool rigidly attached on it. We showed how the same near-hovering controller used for the free flight can be used in contact with the environment to generate a desired contact force. The stability of the system has been then studied and its dependence on the desired 3D force and the

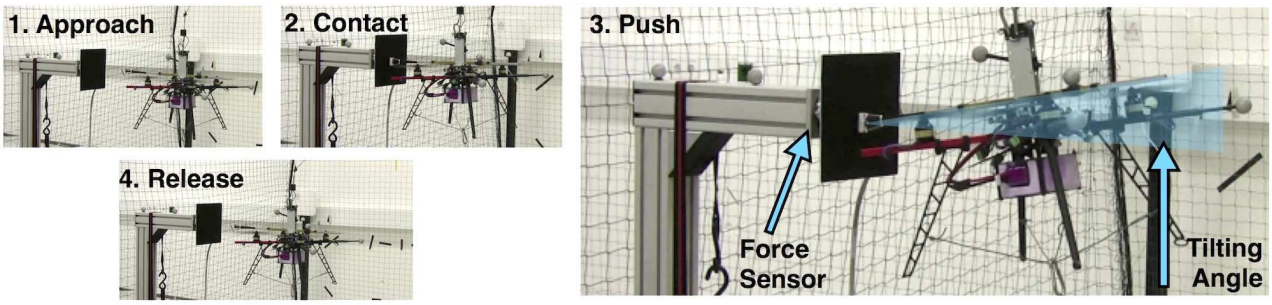

Fig. 5: Snapshots of time series while quadrotor is performing the experiment.

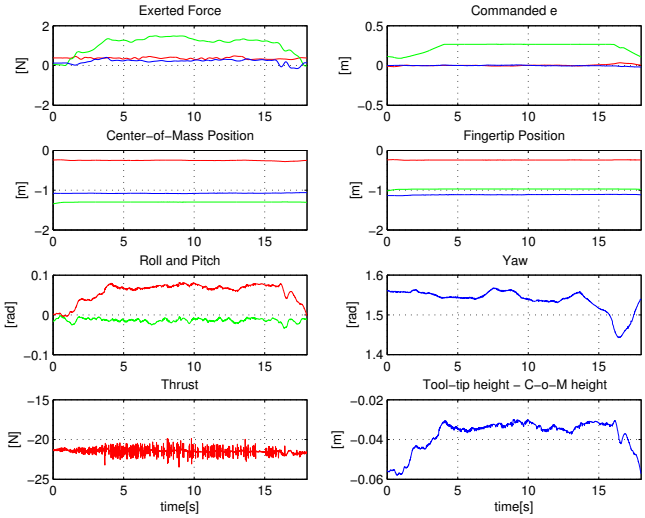

Fig. 6: The main quantities recorded during the performed experiment.

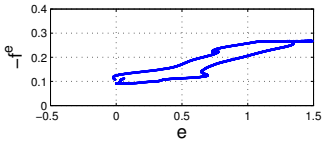

Fig. 7: The relationship between the commanded signal e_1 and the force read from the sensor during the contact phase ($-f_1$).

position of the tool-tip in body frame has been investigated. The presented theory has been validated by preliminary experimental results in which a human operator manually increased and decreased the value of the error component e_1, emulating a "Push and Release" task.

As future work we want to thoroughly study the dynamic case and perform full experiments with an autonomous robot in order to validate the approach in the different interaction cases considered in the paper. The desired interaction forces will be given as input to the system thus fully exploiting the theoretical results derived in Section III.

Acknowledgments

The research leading to these results has received funding from the European Union Seventh Framework Programme FP7/2007-2013 under grant agreement n 601165 of the project WEARHAP WEARable HAPtics for humans and robots.

References

[1] D. J. Lee and C. Ha, "Mechanics and control of quadrotors for tool operation," in *2012 ASME Dynamic Systems and Control Conference*, (Fort Lauderdale, FL), Oct. 2012.

[2] M. Fumagalli, R. Naldi, A. Macchelli, R. Carloni, S. Stramigioli, and L. Marconi, "Modeling and control of a flying robot for contact inspection," in *2012 IEEE/RSJ Int. Conf. on Intelligent Robots and Systems*, (Vilamoura, Portugal), pp. 3532–3537, Oct 2012.

[3] S. Bellens, J. De Schutter, and H. Bruyninckx, "A hybrid pose/wrench control framework for quadrotor helicopters," in *2012 IEEE Int. Conf. on Robotics and Automation*, (St.Paul, MN), pp. 2269–2274, May 2012.

[4] M. B. Srikanth, A. Soto, A. Annaswamy, E. Lavretsky, and J.-J. Slotine, "Controlled manipulation with multiple quadrotors," in *AIAA Conf. on Guidance, Navigation and Control*, (Portland, OR), Aug. 2011.

[5] L. Marconi, R. Naldi, and L. Gentili, "Modeling and control of a flying robot interacting with the environment," *Automatica*, vol. 47, no. 12, pp. 2571–2583, 2011.

[6] B. Yüksel, C. Secchi, H. H. Bülthoff, and A. Franchi, "Reshaping the physical properties of a quadrotor through ida-pbc and its application to aerial physical interaction," in *2014 IEEE Int. Conf. on Robotics and Automation*, (Hong Kong, China), May. 2014.

[7] M. Orsag, C. Korpela, and P. Oh, "Modeling and control of MM-UAV: Mobile manipulating unmanned aerial vehicle," *Journal of Intelligent & Robotics Systems*, vol. 69, no. 1-4, pp. 227–240, 2013.

[8] V. Lippiello and F. Ruggiero, "Exploiting redundancy in cartesian impedance control of UAVs equipped with a robotic arm," in *2012 IEEE/RSJ Int. Conf. on Intelligent Robots and Systems*, (Vilamoura, Portugal), pp. 3768–3773, Oct. 2012.

[9] G. Gioioso, A. Franchi, G. Salvietti, S. Scheggi, and D. Prattichizzo, "Hand driven UAV formation for cooperative grasping and transportation: the flying hand," in *RSS 2013 Work. on Aerial Mobile Manipulation*, (Berlin, Germany), June 2013.

[10] D. Prattichizzo and J. C. Trinkle, "Grasping," in *Springer Handbook of Robotics* (B. Siciliano and O. Khatib, eds.), pp. 671–700, Springer, 2008.

[11] N. Michael, D. Mellinger, Q. Lindsey, and V. Kumar, "The GRASP multiple micro-UAV testbed," *IEEE Robotics & Automation Magazine*, vol. 17, no. 3, pp. 56–65, 2010.

[12] A. Franchi, C. Secchi, H. I. Son, H. H. Bülthoff, and P. Robuffo Giordano, "Bilateral teleoperation of groups of mobile robots with time-varying topology," *IEEE Trans. on Robotics*, vol. 28, no. 5, pp. 1019–1033, 2012.

[13] D. J. Lee, A. Franchi, H. I. Son, H. H. Bülthoff, and P. Robuffo Giordano, "Semi-autonomous haptic teleoperation control architecture of multiple unmanned aerial vehicles," *IEEE/ASME Trans. on Mechatronics, Focused Section on Aerospace Mechatronics*, vol. 18, no. 4, pp. 1334–1345, 2013.

[14] J. J. E. Slotine and W. Li, *Applied nonlinear control*. Prentice Hall, 1991.